Representing Variability and Transmural Differences in a Model of Human Heart Failure

Mohamed M. Elshrif, *Member, IEEE*, Pengcheng Shi, and Elizabeth M. Cherry

***Abstract*—During heart failure (HF) at the cellular level, the electrophysiological properties of single myocytes get remodeled, which can trigger the occurrence of ventricular arrhythmias that could be manifested in many forms such as early afterdepolarizations (EADs) and alternans (ALTs). In this paper, based on experimentally observed human HF data, specific ionic and exchanger current strengths are modified from a recently developed human ventricular cell model: the O'Hara–Virág–Varró–Rudy (OVVR) model. A new transmural HF-OVVR model is developed that incorporates HF changes and variability of the observed remodeling. This new heterogeneous HF-OVVR model is able to replicate many of the failing action potential (AP) properties and the dynamics of both $[Ca^{2+}]_i$ and $[Na^+]_i$ in accordance with experimental data. Moreover, it is able to generate EADs for different cell types and exhibits ALTs at modest pacing rate for transmural cell types. We have assessed the HF-OVVR model through the examination of the AP duration and the major ionic currents' rate dependence in single myocytes. The evaluation of the model comes from utilizing the steady-state (S-S) and S1-S2 restitution curves and from probing the accommodation of the HF-OVVR model to an abrupt change in cycle length. In addition, we have investigated the effect of chosen currents on the AP properties, such as blocking the slow sodium current to shorten the AP duration and suppress the EADs, and have found good agreement with experimental observations. This study should help elucidate arrhythmogenic mechanisms at the cellular level and predict unseen properties under HF conditions. In addition, this AP cell model might be useful for modeling and simulating HF at the tissue and organ levels.**

***Index Terms*—Alternans (ALTs), early afterdepolarizations (EADs), heart failure (HF), O'Hara–Virág–Varró–Rudy (OVVR), remodeling ionic currents.**

I. Introduction

MORE than 15 million Americans suffer from coronary heart disease in the U.S. One-third of them suffer from heart failure (HF) and ∼280 000 die yearly [1]. HF is characterized by decreased contractility and an inability of the ventricles to pump enough blood to the body. At the cellular level, HF is accompanied by remodeling of the ion channels that govern the electrical activity of the heart. During HF, the electrophysiology and the associated arrhythmogenesis mechanisms are altered and this alteration depends on the etiology that led to HF [2]. Therefore, HF cannot be represented by a fixed set of electrophysiological changes. However, there are a number of consistent findings thought to be important for arrhythmogenesis. These include ion channel remodeling, altered calcium homeostasis, and increased accumulated sodium concentration [2], [3]. Many experimental studies observed altered ionic currents and exchangers in failing human ventricular myocytes [4]–[14]. Moreover, noninvasive measurements have confirmed differences in membrane potential and calcium dynamics between failing and nonfailing human hearts [4], [5], with potentially proarrhythmic implications [6], [7].

Recently, O'Hara *et al.* [15] developed a new ventricular AP cell model [O'Hara–Virág–Varró–Rudy (OVVR)] under normal conditions and were able to reproduce many important physiological properties, such as action potential duration (APD) restitution curves. However, the model was not extended to pathological conditions, e.g., HF. Therefore, Mathematical modeling of disease-specific electrical activity of human ventricular cells is a powerful tool that complements the fundamental physiological understanding of remodeling of ionic channels under specific diseases, such as HF, which is observed by experimentalists and can be used to predict complicated situations. There are a few HF ventricular cell models that have been developed for humans [8]–[10], [14], [16], [17], [19]–[24] and different animal species such as canines [11], [12], rabbit [18], and guinea pigs [13]. These models did not include experimentally verified variability in parameter values for the ionic currents and $[Ca^{2+}]_i$ dynamics for cardiac myocytes of the particular species. Therefore, we developed a failing human ventricular cell model using observed variability in ionic current strengths. This new HF-OVVR model is a natural extension of our previously published model [25] for the action potential and calcium dynamics in failing human ventricular myocytes with model improvements, which fall into two categories. First, the new model includes transmural cell types [26], [27]. This will help us to investigate how the heterogeneous remodeling under HF modulates the electrophysiological properties that may lead to arrhythmias [28]. Second, we introduce uncertainties in modified parameter values, which may represent the averages from different HF causes or the variability between isolated myocyte samples from the investigated subject, remodeling ion channel strengths without changing the ionic current kinetics. Therefore, the simulated HF population is constructed by incorporating the upregulation

Manuscript received December 15, 2014; revised March 18, 2015 and May 21, 2015; accepted May 27, 2015. Date of publication June 9, 2015; date of current version July 23, 2015. This work was financially supported by the Libyan-North American Scholarship Program from the Ministry of Higher Education, Scientific Research in Libya, the Ph.D. Program in Computing and Information Sciences at RIT (M. M. E.), and the National Science Foundation under Grant CMMI-1028261 (E. M. C.).

M. M. Elshrif and P. Shi are with the B. Thomas Golisano College of Computing and Information Sciences, Rochester Institute of Technology, Rochester, NY 14623 USA (e-mail: mme4362@rit.edu; spcast@rit.edu).

E. M. Cherry is with the School of Mathematical Sciences, Rochester Institute of Technology, Rochester, NY 14623 USA (e-mail: excsma@rit.edu).

This paper has supplementary downloadable material available at http://ieeexplore.ieee.org.

Color versions of one or more of the figures in this paper are available online at http://ieeexplore.ieee.org.

Digital Object Identifier 10.1109/JBHI.2015.2442833

TABLE I
SUMMARY OF THE CHANGES IN THE MAIN CURRENTS DURING HF AS SUGGESTED BY HF SIMULATION STUDIES

Model	Species	I_{Na}	I_{NaL}	I_{CaL}	I_{to}	I_{K1}	I_{Kr}	I_{Ks}	SERCA	I_{NaCa}	I_{NaK}	I_{Nab}	I_{Cab}	I_{leak}	RyR
Priebe *et al.* [8]	human	–	–	–	–	↓(25%)	–	–	–	↑(65%)	↓(42%)	–	↑(25%)	–	–
Zhang *et al.* [9]	human	↓(57%)	↑(1200%)	↑(200%)	↓(36%)	↓(25%)	–	↓	↓	↑(65%)	↓(42%)	–	↑(25%)	–	–
Trenor *et al.* [10]	human	–	↑(200%)	–	↓(60%)	↓(32%)	–	–	↓(50%)$^{+}$	↑(175%)	↓(10%)	–	↑(153%)	↑(500%)	–
Winslow *et al.* [11]	canine	–	–	–	↓(66%)	↓(32%)	–	–	↓(62%)	↑(75%)	–	–	–	–	–
Zang *et al.* [12]	canine	–	↑(670%)	–	↓(84%)	↓(35%)	–	↓(49%)	↓(85%)	↑(76%)	–	–	–	–	–
Winslow *et al.* [13]	guinea pig	–	–	–	↓(66%)	↓(35%)	–	–	↓(50%)	↑(200%)	–	–	–	–	–
Zlochiver [14]	human	↓(34%)	–	–	↓(36%)	↓(43%)	–	↓(50%)	–	↑(36%)	–	–	–	–	–
Walmsley *et al.* [16]	human	–	–	↑↓(30%)	↑↓(30%)	–	↑↓(30%)	↑↓(30%)	↑↓(30%)	↑↓(30%)	–	–	–	–	–
Shannon *et al.* [17]	human	–	–	–	↓(33%)*	↓(50%)	–	↓(40%)	↓(40%)	↑(200%)	–	–	–	↑(300%)	↑(300%)
Buglisi *et al.* [18]	rabbit	–	–	–	↓(36%)	↓(49%)	–	–	↓(24%)	↑(100%)	–	–	–	–	–
Narayan *et al.* [19]	human	(25–200%)	(25–200%)	–	–	–	–	–	(25%-200%)	-	–	–	–	–	–
Moreno *et al.* [20]	human	–	–	↑(150%)	↓(36%)*	↓(25%)	–	–	↓(36%)	↑(65%)	–	–	–	↓(30%)	–
Lu *et al.* [21]	human	↓(40%)	–	–	↓(64%)	↓(20%)	–	↓(50%)	↓(45%)	↑(65%)	↓(42%)	–	↑	–	↓(50%)$^{\#}$
Gomez *et al.* [22]	human	–	↑(200%)**	–	↓(40%)	↓(68%)	–	–	↓(50%)	↑(175%)	↓(90%)	–	↑(153%)	↑(300%)	–
Moreno *et al.* [23]	human	–	↑(1000%)	–	↓(36%)*	↓(25%)	–	–	↓(36%)	–	↓(10–42%)	↑(1600%)	–	↑(350%)	–

+ Trenor *et al.* [10] EC_{50SR} ↓(11%). * Shannon *et al.* [17] $I_{to_{\mathrm{slow}}}$ ↓(35%). # Lu *et al.* [21] ↑(23%). Gomez *et al.* [22] ** $\mathrm{tau}_{h\,L}$ ↑(200%).

or downregulation of transmembrane current conductances as observed in experiments (see Table II).

In the present study, first, the electrophysiological activity of a transmural single myocyte was simulated using well-justified modifications of a recent mathematical model of the human ventricular AP [15] to replicate the experimentally reported human HF phenotypes. Second systematic and quantitative variability in ionic currents and exchangers was introduced utilizing experimental observations published in the literature.

II. RELATED WORK

There are several simulation studies [8]–[14], [16]–[24] that aimed to simulate remodeled AP properties during HF. The adapted alterations of the transmembrane currents from these simulation studies are summarized in Table I. We will explain the remodeled currents of these HF models and the impact of each altered current on the HF model.

For the fast sodium current I_{Na}, most previous HF simulation studies on a single myocyte [8], [10]–[13], [16]–[18], [20], [22], [23] did not consider remodeling I_{Na} in their HF models, except a few studies that consider a reduction of I_{Na} [9], [14], [21] by ↓57%, 34%, and 40%, respectively. In addition, one study [19] considered scaling I_{Na} by 25–200% from the control value. Reducing I_{Na} will affect the amplitude as well as the upstroke velocity of an action potential.

Regarding the late sodium current I_{NaL}, the preceding simulation studies [8], [11], [13], [14], [16]–[18], [20], [21] did not consider remodeling I_{NaL} in their HF models. However, more recent HF simulation studies [9], [10], [12] [19], [22], [23] believed that remodeling the I_{NaL} plays a dominant role in changing AP characteristics during the plateau and repolarization phases, and as a consequence, this current could alter the duration of an AP. I_{NaL} is remodeled in these simulation studies through increasing the peak current density 12-fold in [9], 2-fold in [10], 6.7-fold in [12], 0.25-2-fold in [19], 2-fold in [22], and 10-fold in [23].

The former simulations of HF cell models did not consider altering the L-type calcium current I_{CaL} [8], [10]–[14], [17]–[19], [21]–[23], except three studies [9], [16], [20] that remodeled I_{CaL} by ↑200%, ↑↓30%, and ↑150%, respectively.

Previous HF simulation studies show agreement regarding the transient outward current I_{to}. Most of these studies reduced I_{to} in human by ↓33% [17], ↓36% [9], [14], [20], [23], ↓40% [22], ↓60% [10], and ↓64% [21]. For animal species, I_{to} is reduced by ↓36% [18] in rabbit, ↓66% and ↓84% in canine [11], [12], and ↓66% in guinea pig [13] myocytes. Two HF models did not change I_{to} [8], [19]. One study [16] perturbed I_{to} in both directions by ↑↓30%.

Most of the existing simulation studies follow the findings that show downregulation of the inward rectifier potassium current I_{K1} by implementing a reduction of I_{K1} density between ↓25% and 68% in their HF models [8]–[13] [14], [17], [18], [20]–[23]. Two HF studies [16], [19] used the same I_{K1} as in normal conditions.

Surprisingly, none of the previous simulation studies [8]–[14], [17]–[23] considered remodeling the rapid delayed rectifier potassium current I_{Kr} in their HF cellular models to investigate the effects of this current on AP characteristics. Only one study [16] considered investigating the effect of I_{Kr} by ↑↓30%.

Similarly, most previous HF simulation models [8], [10], [11], [13], [18]–[20], [22], [23] did not investigate remodeling the slow delayed rectifier potassium current I_{Ks}. However, there are a few studies [9], [12], [14], [16], [17], [21] that integrated a reduction of I_{Ks} within the range ↓30–50%. One study [9] did not specify the percentage reduction in I_{Ks} density used in the paper.

In addition, many HF studies [10]–[14], [17], [18], [20]–[23] remodeled the sarcoplasmic reticulum calcium SERCA activity ranging from ↓24% to 85%, along with one study [9] which did

TABLE II
SUMMARY OF THE REMODELED CURRENTS AND EXCHANGERS OF THE HF-OVVR MODEL IN A SINGLE MYOCYTE EXPRESSED AS MEAN ± STANDARD DEVIATION ($\mu \pm$ SD)

Current	Transmural Heart Failure Remodeling			Experimental Observations	References
	Epicardial	Midmyocardial	Endocardial		
I_{Na}	↓(62.6 ± 11.5%)	↓(62.6 ± 11.5%)	↓(62.6 ± 11.5%)	↓39.3 ± 6.5% – ↓91.1 ± 9.3%	[29]–[31]
I_{NaL}	↑(93.3 ± 10.1%)	↑(93.3 ± 10.1%)	↑(93.3 ± 10.1%)	↑30.0 ± 0% – ↑238.5 ± 1.3%	[29], [32]–[34]
I_{CaL}	unchanged	unchanged	unchanged	unchanged	[35]–[45]
I_{to}	↓(40.4 ± 8.7%)	↓(37.6 ± 3.3%)	↓(50.8 ± 2.0%)	↓26.4 ± 1.3% – ↓73.2 ± 5.8%	[39], [42], [45]–[50]
I_{K1}	↓(55.3 ± 13.9%)	↓(52.7 ± 14.8%)	↓(55.0 ± 16.1%)	↓40 ± 0% – ↓64 ± 0%	[39], [42], [45], [46], [51]–[54]
I_{Kr}	↓(45.9 ± 9.5%)	unchanged	↓(27.3 ± 1.7%)	↓27.3 ± 1.7% – ↓51.0 ± 0%	[50], [54]–[56]
I_{Ks}	↓(59.4 ± 2.1%)	↓(49.5 ± 1.6%)	↓(57.7 ± 2.2%)	↓49.5 ± 1.6% – ↓61.7 ± 1.4%	[45], [54]–[57]
I_{NaCa}	↑(131.4 ± 62.8%)	↑(131.4 ± 62.8%)	↑(131.4 ± 62.8%)	↑80.0 ± 0% – ↑200.0 ± 0%	[58]–[61]
I_{NaK}	↓(40.2 ± 15.5%)	↓(40.2 ± 15.5%)	↓(40.2 ± 15.5%)	↓36.0 ± 0% – ↓56.0 ± 0%	[62]–[66]
SERCA	↓(41.3 ± 12.5%)	↓(42.3 ± 11.3%)	↓(41.1 ± 10.1%)	↓15.4 ± 10% – ↓65.0 ± 7%	[5], [27], [61], [67]–[74]

Some of the data used in remodeling ionic currents are animal data.

not specify the percentage of reduction. One study [19] scaled SERCA by 25–200% from the original value. In addition, one study [16] considered perturbing SERCA activity by ↑↓30%. One sole study [8] did not consider remodeling SERCA.

On the contrary, most of the preceding HF simulation models realized the importance of incorporating remodeling of the sodium calcium exchanger I_{NaCa}. Therefore, an upregulation was incorporated with a broad range of ↑36% to 200% in these HF models [8]–[14], [17], [18], [20]–[22]. One study [16] perturbed I_{NaCa} by ↑↓30%. Also, two studies [19], [23] did not consider remodeling this current in their HF models.

For the sodium–potassium pump $\mathrm{Na}^+/\mathrm{K}^+$, some of the HF cellular models incorporated remodeling I_{NaK} through reducing its conductance (G_{NaK}) by ↓10% [8] and ↓42% [9], [10], [21]. One study [23] chose to use the range of these previous studies, ↓10–42%. In addition, one study [22] remodeled I_{NaK} by ↓90%, while the rest of the HF models [11]–[14], [16]–[20] did not remodel this pump.

Regarding background currents, most of the previous HF models did not change the sodium background current I_{Nab}, except one study [23], which increased I_{Nab} 16-fold. However, some of these HF studies [8], [9] altered the calcium background current I_{Cab} by ↑25%, while studies [10], [22] altered this current by ↑153%. One study [21] did not specify the percentage of remodeling I_{Cab}.

For I_{leak}, many of the previous HF models [8], [9], [11]–[14], [16], [18], [19], [21], [24] did not consider remodeling this current. However, a few studies [10], [17], [20], [22], [23] increased this current with disparate percentages of ↑500%, 300%, 30%, 300%, and 350%, respectively. In addition, two studies [17], [21] considered remodeling the ryanodine receptor (RyR), but with opposite direction of remodeling. One study [17] incorporated an increase of RyR activity by ↑300%, while [21] considered a reduction of RyR activity by ↓50%.

Concerning remodeling heterogeneous cell types, most of the previous HF models [8]–[11], [13], [14], [16]–[21], [23] remodeled a single cell type, except for two studies [12], [22], which considered remodeling three transmural types of cells. One of these studies [12] did not remodel the statistical difference between cell types during HF as observed experimentally, instead, it used the same remodeling parameters setting across all types of cells. In addition, the other [22] considered remodeling only two types of ionic currents: I_{NaCa} and I_{SERCA}.

Most importantly, most of the previous HF models [8], [9], [11]–[14], [17], [18], [20]–[23] incorporated a fixed set of remodeled current, exchanger, and pump parameter values without introducing any kind of uncertainty to the remodeling parameters. However, a few studies [10], [19] considered different ways of including uncertainty. One study [19] scaled the sarcoplasmic reticulum calcium uptake current I_{up} by 25–200% as well as the time constants of fast and slow sodium channel inactivation $\tau_{h,j}$ by the same scale. In addition, Trenor *et al.* [10] performed a sensitivity analysis of ionic currents by ±15% to assess the sensitivity of electrophysiological biomarkers to changes in ionic current properties. Another study [16] generates a population for both normal and HF cellular models through perturbing the G_{CaL}, G_{to}, G_{K1}, G_{Kr}, G_{Ks}, G_{NaCa}, and J_{up} ionic parameters by ±30%.

III. METHODS

A. OVVR Cellular Electrophysiology Model Description

In this study, the following differential equation was used to describe the time-dependent electrophysiological behavior of a single normal myocyte [15]:

$$dV_m/dt = -(I_{\mathrm{ion}} + I_{\mathrm{stim}})/C_m \tag{1}$$

where V_m is the transmembrane voltage; t is time; I_{ion} is the total of all transmembrane ionic currents, pumps, and exchangers; I_{stim} is an external stimulus current; and C_m is the cell membrane capacitance. Furthermore, I_{ion} can be represented by the following equation:

$$I_{\mathrm{ion}} = I_{\mathrm{Na}} + I_{\mathrm{NaL}} + I_{\mathrm{CaL}} + I_{\mathrm{CaK}} + I_{K1} + I_{Kr} + I_{Ks} + I_{\mathrm{to}} + I_{\mathrm{NaCa}} + I_{\mathrm{NaK}} + I_{\mathrm{Nab}} + I_{\mathrm{Cab}} + I_{Kb} + I_{p\mathrm{Ca}}. \tag{2}$$

This original undiseased OVVR model was evaluated through the steady-state (S-S) rate dependence and restitution curves of an action potential in a single myocyte based on data from more

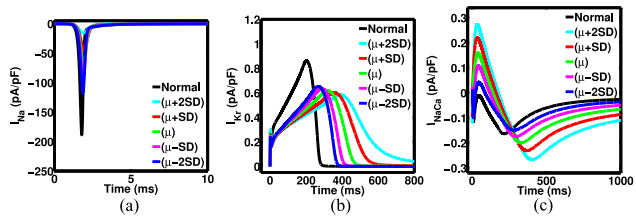

Fig. 1. Simulated (a) I_{Na}, (b) I_{Kr}, and (c) I_{NaCa} under normal conditions OVVR (black lines) and HF conditions HF-OVVR expressed as mean ± 2SD of the endocardial cell type at CL=1000 ms.

than one hundred normal human hearts. In addition, it presents new formulations for unavailable measurements of I_{CaL}, potassium currents, and I_{NaCa}. However, the model was not formulated to investigate disease-specific situations such as HF, which is our aim in the present manuscript.

B. Developed HF-OVVR Cellular Electrophysiology Model Description

Certain ionic exchanger and pump currents were investigated with their corresponding experimental human HF data published and remodeled based on these observations. We used the same equations of the normal OVVR model [15] and reformulated the maximum current conductances for major currents of the undiseased OVVR model [15], while other values remained unchanged, such as the background currents. We take the first steps toward developing a meaningful representation of population variability through calculating the mean and the standard deviation (SD) for each ionic current across experimental observations found in the literature. Table II summarizes the heterogeneous remodeled ionic currents used in our HF-OVVR model along with the data sources. The details of HF remodeling for each current we are discussed below.

1) *Fast sodium current (I_{Na}):* This current is activated during the depolarization phase of an AP, which is responsible for upstrokes during the normal impulses in a single myocyte. Most experimental studies on HF-affected myocytes show that the peak I_{Na} is decreased in a range from ↓39.3 ± 6.5% to ↓91.1 ± 9.3% [29]–[31], except for one study [75], which indicates that the peak I_{Na} is unchanged from normal levels. We calculated the mean (μ) and SD of observed remodeling of I_{Na} in cardiomyocytes isolated with these recent experimental studies [29]–[31]. In our simulations, we use (μ ± 2SD) to express the range of variations. Fig. 1(a) shows the simulated reduction of the I_{Na}.
2) *Late sodium current (I_{NaL}):* The participation of this current is during the plateau and repolarization phases, not during the depolarization phase of an AP due to its slow dynamics. Most experiments on HF human myocytes [29], [32]–[34] show that the I_{NaL} density is increased within a range from ↑30.0 ± 0% to ↑238.5 ± 1.3%. However, one study [76] showed similar INaL densities in failing and normal hearts, although the small sample size did not allow a statistically significant comparison. Therefore, we computed the average of these experimental observations in human HF myocytes from [29], [32]–[34] considering the variation between these studies.
3) *L-type calcium current (I_{CaL}):* This current plays an essential role in shaping the AP morphology, especially in the long plateau phase. Also, it initiates the excitation-contraction coupling. The majority of previous HF observations report that there is no significant difference between I_{CaL} in failing and non-failing myocytes [35]–[45]. However, one study [51] observed a decrease in the dihydropyridine binding sites within a range from ↓35% to 48% and mRNA by ↓47%. We decided to use the same I_{CaL} density as in nonfailing myocytes as reported by most of these experiments for all cell types.
4) *Transient outward potassium current (I_{to}):* This current impacts the notch portion during the rapid phase 1 repolarization of an AP. It is agreed across most experimental observations on human ventricular species that I_{to} is decreased with a range from ↓26.4 ± 1.3% to ↓73.2 ± 5.8% under HF conditions [39], [42], [45]–[50], [77]. However, these studies claim that there is no significant change in the kinetics of I_{to} in failing myocytes when compared with non-failing myocytes. Therefore, we chose to incorporate a downregulation of I_{to} under HF conditions heterogeneously. This means that different outward potassium conductance settings (G_{to} values) are used to model the transmural heterogeneity of cardiac ventricular cells based on the previous experimental observations [45], [49], [50], [77] for epicardial cells, [39], [42], [46], [47], [50] for midmyocardial cells, and [48]–[50], [77] for endocardial cells. As a consequence, I_{to} is reduced by ↓40.4 ± 8.7%, ↓37.6 ± 3.3%, and ↓50.8 ± 2.0% for epicardial, midmyocardial, and endocardial cell types, respectively.
5) *Inward rectifier potassium current (I_{K1}):* I_{K1} plays a significant role in stabilizing the resting membrane potential (RMP) and in shaping the last portion of the repolarization phase of an AP [78]. Observations from numerous studies have shown that I_{K1} is significantly downregulated within a range from ↓40 ± 0% to ↓64 ± 0% [39], [42], [45], [46], [51]–[54]. Hence, we adopted a reduction of the peak I_{K1} by reducing its conductance (G_{K1}) heterogeneously, after calculating the mean and SD, by ↓55.3 ± 13.9%, ↓52.7 ± 14.8%, and ↓55.0 ± 16.1% for epicardial, midmyocardial, and endocardial cell types, respectively. The transmural remodeling is based mainly on the experimental observations from [39], [45], [51], [52] for epicardial, [39], [46], [51], [52] for midmyocardial, and [39], [51], [52] for endocardial cells.
6) *Rapid delayed rectifier potassium current (I_{Kr}):* I_{Kr} plays an important role in the repolarization phase of an AP. This current has been studied extensively with controversial observations. Many experiments observed a reduction within a range from ↓27.3 ± 1.7% to ↓51 ± 0% [50], [54]–[56], but some studies [42], [45], [79] indicated that I_{Kr} is unchanged. This controversial observation is due in part to the cell type investigated.

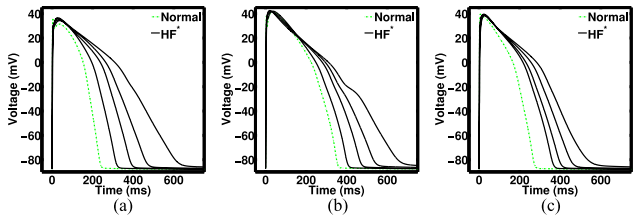

Fig. 2. Representative variation of the simulated OVVR action potentials under normal (dotted green) and different HF (solid black) conditions for (a) epicardial, (b) midmyocardial, and (c) endocardial cell types. (*) The four black solid lines represent different variations in parameter values of μ-$2SD$, μ-SD, μ, and μ+SD for all ionic currents at a CL of 1000 ms.

Therefore, we decided to incorporate remodeling of this current based on the cell type, due to the differences in the shape and duration of APs between these cells, by $\downarrow 45.9 \pm 9.5\%$ for epicardial cells [50], unchanged for midmyocardial cells [42], [45], [79], and $\downarrow 27.3 \pm 1.7\%$ for endocardial cells [50]. The simulated I_{Kr} current traces are shown in Fig. 1(b).

7) *Slow delayed rectifier potassium current (I_{Ks}):* I_{Ks} is a slow activating current that affects the last portion of repolarization of an AP. Most of the former studies show an agreement on the downregulation of I_{Ks} within a range from $\downarrow 49.5 \pm 1.6\%$ to $\downarrow 61.7 \pm 1.4\%$ [45], [54], [57]. Only one study [80] exhibits that the KCNE1 mRNA increases by $\uparrow 25\%$. We decided to follow the majority of the previous experimental observations through reducing the peak current density of I_{Ks} heterogeneously by $\downarrow 59.4 \pm 2.1\%$ [45], [57], $\downarrow 49.5 \pm 1.6\%$ [57], and $\downarrow 57.7 \pm 2.2\%$ [57] for epicardial, midmyocardial, and endocardial cell types, respectively.
8) *Sodium–calcium exchanger current (I_{NaCa}):* I_{NaCa} supports regulating the intracellular calcium concentration. Many experimental observations on the myocardium of HF patients found that the measured activity of the $\mathrm{Na}^+/\mathrm{Ca}^{2+}$ exchanger is modified with a wide range from $\uparrow 80.0 \pm 0\%$ to $\uparrow 200.0 \pm 0\%$ compared to nonfailing myocytes [58]–[61], [81]. Therefore, a homogeneous upregulation of I_{NaCa} by $\uparrow 131.4 \pm 62.8\%$ for all different cell types is incorporated into the undiseased OVVR model, which includes both the membrane I_{NaCa_i} and subspace $I_{\mathrm{NaCa}_{ss}}$. Fig. 1(c) exhibits the simulation results of the modified I_{NaCa}.
9) *Sodium–potassium pump current (I_{NaK}):* I_{NaK} maintains the RMP and ionic homeostasis inside the cell. The majority of experimental studies report that $\mathrm{Na}^+/\mathrm{K}^+$ pump activity is downregulated within a range from $\downarrow 36 \pm 0\%$ to $\downarrow 56 \pm 0\%$ [62]–[66]. One study [82], observed a non-significant decrease of $\downarrow 10\%$. We decreased the peak of I_{NaK} homogeneously by $\downarrow 40.2 \pm 15.5\%$ in our HF-OVVR cellular model.
10) *Sarcoplasmic reticulum Ca^{2+} (*SERCA*) pump:* This pump transports calcium ions from the cytosol into the SR. Most of the experimental observations claim that an alteration of $[Ca^{2+}]_i$ in failing human and animal myocytes is based on the dynamics of the SR Ca^{2+} pump, which is decreased in a range from $\downarrow 15.4 \pm 0\%$ to $\downarrow 50.0 \pm 0\%$ [5], [27], [61], [67]–[74]. $[Ca^{2+}]_i$ under HF conditions is characterized by a reduction of calcium levels during the systolic phase, an elevation of calcium levels during the diastolic phase, and prolongation of calcium levels during the relaxation phase. We decided to incorporate a remodeling of SERCA in our HF-OVVR model through decreasing the SERCA activity heterogeneously by $\downarrow 41.3 \pm 12.5\%$ [5], [27], [61], [67], [68], [71], [72], $\downarrow 42.3 \pm 11.3\%$ [27], [61], [67], [68], [71], [72], [74], and $\downarrow 41.1 \pm 10.1\%$ [5], [27], [61], [67], [68], [71]–[73] for epicardial, midmyocardial, and endocardial cell types, respectively.

C. Experimental Data

1) *Data sources:* Most of the sources of experimental data used to construct and simulate human HF myocyte are based mainly on human species. However, due to the scarcity of data on humans for some currents during HF, we benefit from the existence of data from other animal species found in the literature. Therefore, we incorporated canine [54], [57], [79] and rabbit [55], [56], [78] data.
2) *Data variability:* Data for the HF-OVVR model are presented as the mean $\pm$ SD ($\mu \pm SD$). We calculate the SD in this manuscript based on the formula $\sqrt{\sigma_1^2 + \sigma_2^2 + \cdots + \sigma_n^2}$, where σ_i^2 is the variance of the instance i and n is the number of experiments involved in the calculations of the specified remodeling current.
3) *Biomarkers calculation:* We varied each modified parameter from $(\mu + 2SD)$ to $(\mu - 2SD)$ in increments of 1 SD and calculated the biomarkers for each varied parameter value. For each biomarker, the minimum and maximum biomarker values obtained over all parameter variations and over all currents are given as the range in Table III.

D. Measurement of Restitution Curves and Accommodation

In order to study how the cycle length (CL) perturbation affects the ventricular APD, two common protocols were implemented: steady-state restitution (S-S), and S1-S2 restitution, along with probing the accommodation of APD to a single change in CL. For every protocol, we generated APs using a current strength twice diastolic threshold at a CL of 1000 ms. APDs were assessed by measuring the repolarization voltage thresholds corresponding to 90% (APD_{90}) and 50% (APD_{50}) after pacing for 1 min at the corresponding CL.

For the steady-state protocol, the targeted myocyte was stimulated for 1 min beginning from a CL of 1000 ms, after which the CL was decreased in steps until 2:1 block was observed. For every CL, the last APD and the prior diastolic interval (DI) pair were recorded. However, when the targeted myocyte exhibited alternans (ALTs) during pacing process, the last two DI and APD were registered.

For the S1-S2 protocol, the intended myocyte was stimulated for 1 min with a constant CL, which is known as S1, after which

TABLE III
COMPARISON BETWEEN EXTRACTED ELECTROPHYSIOLOGICAL BIOMARKERS FROM THE SIMULATIONS OF THE OVVR MODEL UNDER NORMAL AND HF CONDITIONS FOR TRANSMURAL CELL TYPES

Biomarker	Normal			Heart Failure		
	epi	midmyo	endo	epi	midmyo	endo
APD_{90} (ms)	229.7	345.0	262.3	306.9–590.7	392.8–628.8	352.2–512.2
APD_{50} (ms)	187.6	281.3	207.6	249.0–436.9	318.3–466.4	277.7–373.1
Triangulation (ms)	42.1	63.7	54.7	57.9–153.8	74.5–162.4	74.5–139.1
RMP (mV)	−87.8	−87.6	−87.9	−87.8–86.5	−87.5–85.8	−87.8–86.5
Amplitude (mV)	123.2	125.5	127.5	117.3–118.6	122.5–124.1	122.8–124.1
V_{notch} (mV)	27.8	28.6	–	30.0	35.0	–
$V_{plateau}$ (mV)	31.4	41.3	37.6	34.3–39.1	41.7–42.6	38.2–39.6
$(dV/dt)_{max}$ (V/s)	217.1	213.2	220.7	53.0-149.0	52.1–145.7	48.1–150.4
$Restitution\ MA_{APD}$ (ms)$^+$	21.9	24.0	26.2	14.7–55.0	16.4–23.6	20.9–40.3
$Restitution\ CL_{min}$ (ms)$^+$	165.0	270.0	200.0	225.0–500.0	300.0–525.0	270.0–600.0
$Restitution\ DI_{min}$ (ms)$^+$	1.28	4.02	3.68	1.9–16.7	0.2–15.9	1.3–23.3
$Restitution\ Max.\ slope^+$	0.36	0.21	0.54	0.26–0.60	0.23–0.70	0.28–0.86
$Alternans\ onset\ CLs\ range$ (ms)$^+$	165.0	–	280.0–200.0	480.0–225.0	600.0–420.0	380.0–270.0
$Alternans\ magnitude$ (ms)$^+$	1.5	–	12.0–3.0	12.3–0.4	36.0–0.5	20.6–1.9
$EADs\ CLs\ range$ (ms)$^+$	–	–	–	2000.0–1700.0	2000.0–850.0	2000.0–1900.0
APD_{90} in the $EADs\ regime$ (ms)*	–	–	–	1245.4–865.8	886.4–805.5	1254.3–801.8
$[Ca^{2+}]_i\ 50\%\ decay$ (ms)	178.4	169.1	297.1	217.0–859.5	233.7–693.6	414.8–529.4
$[Ca^{2+}]_i\ systolic\ amplitude$ (μM)	697.4	1031.0	401.5	193.3–627.8	255.7–793.6	267.5–352.3
$[Ca^{2+}]_i\ time\ to\ peak$ (ms)	41.5	32.3	55.4	44.7–175.5	47.6–181.7	64.9–168.5
$[Ca^{2+}]_i\ diastolic\ steady\ state$ (μM)	77.1	92.8	87.4	82.1–89.3	94.1–96.8	94.8–99.1
$[Na^+]_i\ peak$ (ms)	7.7	8.2	7.5	7.8–8.7	8.4–9.4	7.8–9.0

The pacing CL= 1000 ms. + Downsweep pacing protocol was used starting from CL= 1000 ms. $*$ For EADs, the pacing protocol begins at CL= 2000 ms.

a second stimulation (S2) was used after a variable DI. The last pair of DI and APD were recorded. The amplitude of short-term memory (STM) was computed as the variation between APD values for the maximum DI at the highest S1 CL, which is in our simulations 1000 ms, and the lowest S1 CL before block or ALTs was noticed [83].

In addition, we adapted a protocol for measuring the accommodation of APD to an abrupt change in CL, since this protocol was recommended as a clinical marker for arrhythmia risk [84]. We follow the same procedure from the preceding studies [85], [86] to construct the accommodation curve by recording APD_{90} at a CL of 1 s after pacing for 8 min, after which the CL was abruptly decreased to 600 ms for a similar pacing period (8 min). Then, the CL was restored to 1 s for another 8 min pacing period (for more details, see [25] and [87]).

In addition, it is worth mentioning that the stable steady-state is difficult to achieve when implementing cellular models. We paced the HF-OVVR cellular model for 5 min at a fixed CL after which we measured the difference between the last two consecutive APDs and found it to be 10^{-4} ms.

E. Numerical Algorithms

Time derivatives were integrated uniformly using the explicit Euler method to solve the ordinary differential equations of the AP and concentration dynamics of the cellular model. The integration of the ionic gating variables was implemented using the Rush and Larson method [88]. The time resolution used for the HF-OVVR was 0.02 ms, with the calcium equations integrated with a smaller time step of 0.001 ms. All single-variable functions were pre-computed and saved in lookup tables [89] to reduce the computational time. Action potentials were stimulated using a transmembrane stimulus current 32.0 μA/μF for 2.0 ms.

All simulations were written in Fortran 95, visualized using MATLAB, and run on a MAC Pro 2×2.8 GHz Quad-Core Intel Xeon CPU with 32-GB 800-MHz DDR2 FB-DIMM RAM. It took 1.3 min to simulate 60 s of physical time and performing the whole simulation for each cell type under one set of conditions took 2.2 h.

IV. RESULTS

A. HF Simulation of an AP in Transmural Cells

Fig. 2 depicts the transmural simulated APs of the normal OVVR model (dotted green lines) and HF-OVVR model (solid black lines) for epicardial (a), midmyocardial (b), and endocardial (c) cell types at CL 1000 ms. As shown in the left panel of Fig. 2, the HF settings of the OVVR model diminish the spike-and-dome morphology of an epicardial AP and the plateau is increased. In addition, APD_{90} is increased due to the slow repolarization dynamics. Similar behavior is observed in the failing midmyocardial cell type (see the middle panel of Fig. 2), where APD_{90} is increased. Some HF population cases exhibit a two-phase repolarization, which also has been observed experimentally [37]. For the failing endocardial cell type (see the left panel of Fig. 2), the maximum amplitude is unchanged, but the AP gets delayed due to the reduction of I_{Na} for all of the HF population. Table III summarizes all the extracted biomarkers of the OVVR model under undiseased and HF conditions for heterogeneous cell types.

B. Rate Dependence of APD and Major Currents

An important role in excitation is the adaptation of an AP to changes in pacing CL. As illustrated in Fig. 3(a) and (b), the APs of the HF-OVVR model exhibit stronger rate dependence than

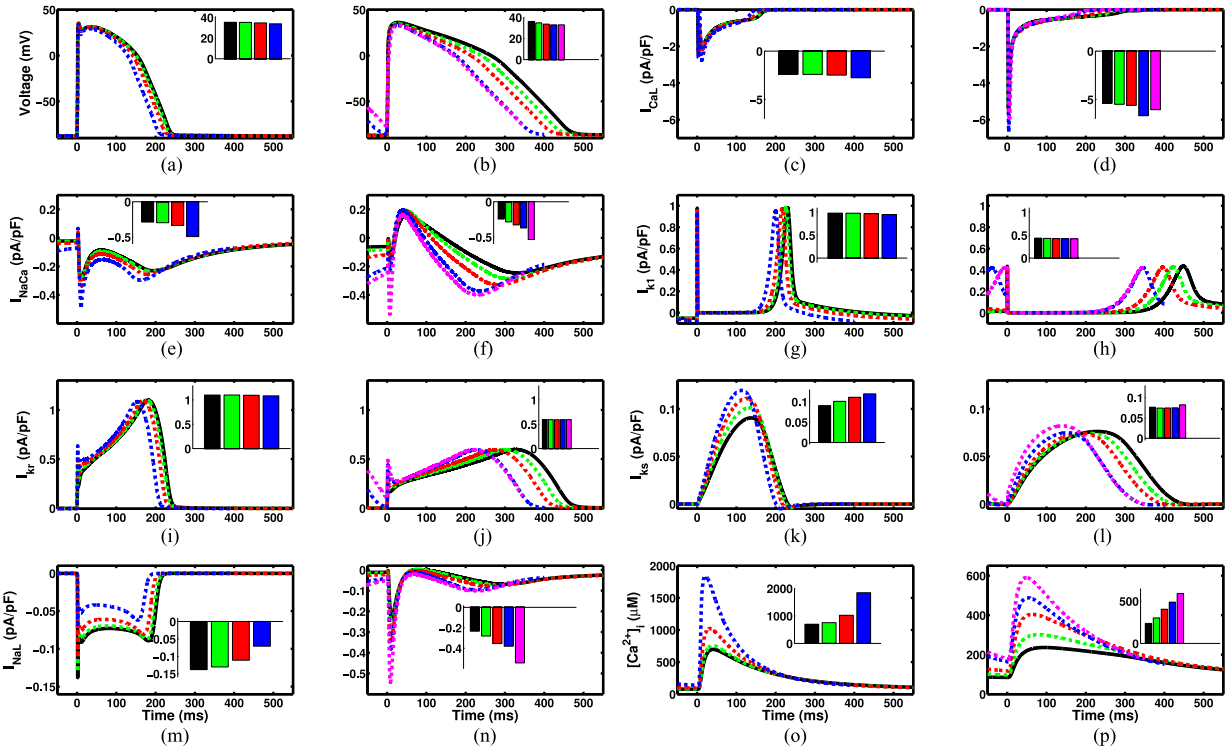

Fig. 3. Rate dependence of action potentials, primary transmembrane currents, and intracellular calcium concentration in a single myocyte for the normal OVVR (columns 1 and 3) and HF-OVVR (columns 2 and 4) models for CLs of 1000 ms (solid black), 800 ms (dashed green), 600 ms (dashed red), 400 ms (dashed blue), and 350 ms (dashed purple). The HF-OVVR model generally shows more rate dependence; however, the normal OVVR model shows greater rate dependence for I_{Ks} and $[Ca^{2+}]_i$. The inset bar diagrams indicates the peak values for each specific curve (a) Normal OVVR Ep (b) HF-OVVR Epi (c) Normal OVVR Epi (d) HF-OVVR Epi (e) Normal OVVR Epi (f) HF-OVVR Epi (g) Normal OVVR Epi (h) HF-OVVR Epi (i) Normal OVVR Epi (j) HF-OVVR Epi (k) Normal OVVR Epi (l) HF-OVVR Epi (m) Normal OVVR Epi (n) HF-OVVR Epi (o) Normal OVVR Ep (p) HF OVVR Epi.

APs of the OVVR model. For I_{CaL}, the HF-OVVR also exhibits stronger rate dependence than the OVVR model. However, the maximum amplitude in the HF-OVVR is two times larger than in the OVVR model for all CLs; see Fig. 3(c) and (d). Due to the reduction of SERCA, the systolic calcium amplitude is reduced and contributes to the slow diastolic decay of calcium, which induces more calcium influx during the AP plateau phase. Similar rate adaptation is observed for I_{NaCa}, where the HF-OVVR model possesses stronger rate adaptation than the OVVR model, as shown in Fig. 3(e) and (f). Regarding I_{K1}, both models exhibit limited rate dependence, as depicted in Fig. 3(g) and (h), but the OVVR model possesses maximum values larger than the HF-OVVR model by $\sim$100%. For I_{Kr}, both models show limited rate dependence with the HF-OVVR model peak current values smaller than the OVVR model by $\sim$50% for all CLs; see Fig. 3(i) and (j). For I_{Ks}, the OVVR model exhibits larger rate dependence than the HF- OVVR model. As shown in Fig. 3(k) and (l), the maximum value is increased as the CL is decreased for the OVVR model, but it is slightly decreased for the HF-OVVR model before it is increased at shorter CLs. In contrast, the HF-OVVR model has stronger rate dependence for I_{NaL} than the OVVR model at shorter CLs; see Fig. 3(m) and (n). Both models exhibit large rate dependence of the calcium transient for all CLs, as shown in Fig. 3(o) and (p). However, the OVVR model has a peak calcium value four times larger than that of the HF-OVVR model.

C. Restitution Curves and STM

Fig. 4 (dashed lines) shows S1-S2 APD restitution curves for a range of S1 CLs for the HF-OVVR model. These S1-S2 curves are superimposed with S-S APD restitution curves. All HF-OVVR restitution curves decrease monotonically with CL. Also, all transmural cell types exhibit STM with the midmyocardial cell possessing the largest STM = 23.6 ms, and the epicardial cell having the lowest, STM = 14.7 ms. The endocardial cell falls in between with STM = 20.9 ms. Fig. 5 exhibits the time course (24 min) of APD adaptation to an abrupt decrease and increase of CL for both the normal OVVR and HF-OVVR models. When accommodating to a decrease in CL, the HF-OVVR model for the epicardial cell type has two phases of accommodation. In the first phase, the APD has a rapid decrease and increase in the AP duration followed by slow decay until it reaches a steady state. However, for the normal epicardial cell type of the OVVR model, the APD is consistently decreasing. Similar behavior was observed for accommodation to an increase in CL; see Fig. 5.

D. Alternans

ALTs occurs for all three types of cells of the HF-OVVR model, but with a different ALTs window and magnitude. For epicardial cells [see Fig. 6(a) and (b)], the ALTs onset occurs at a CL of 400 ms and lasts to a CL of 350 ms with a maximum ALTs

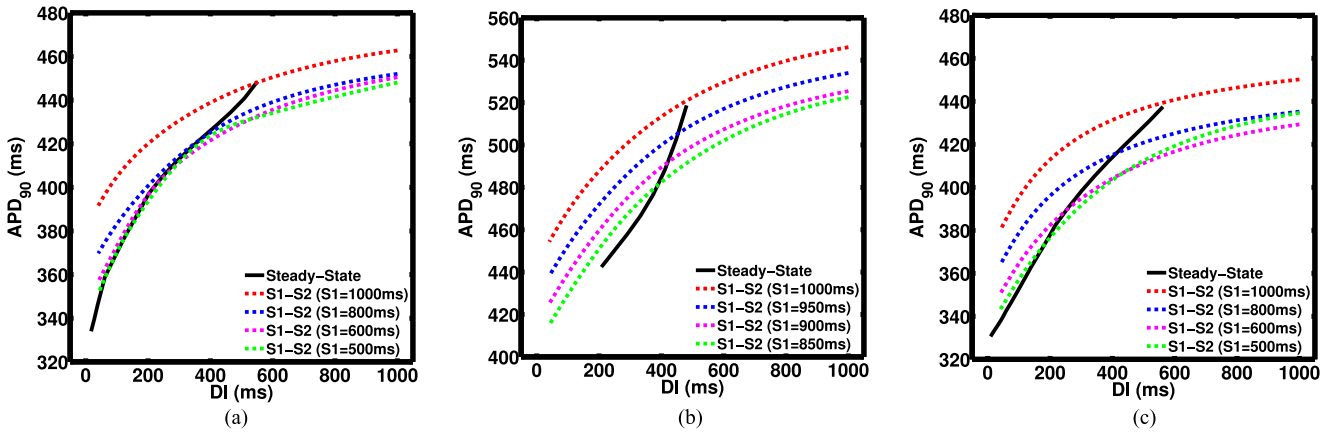

Fig. 4. Steady-state (black lines) and S1-S2 (dotted lines) APD restitution curves for the HF-OVVR model in a single myocyte: (a) epicardial. (b) midmyocardial. (c) endocardial. Curves were obtained after pacing for 60 s and show significant differences among the cell type.

amplitude of ∼30.0 ms. As shown in Fig. 6(c) and (d), which represents the midmyocardial cell, the ALTs window is 420–600 ms with ∼36.0 ms maximum APD_{90} difference. The endocardial cell type, as depicted in Fig. 6(e) and (f), has the lowest ALTs amplitude (∼22.0 ms) along with the lowest ALTs onset CL of 380 ms. The ALTs window falls between 270 and 380 ms.

E. Early Afterdepolarizations (EADs)

Usually, ventricular arrhythmias and sudden cardiac death are associated with HF [90], and EADs are thought to play a major role in the initiation of arrhythmias. As depicted in Fig. 7, the HF-OVVR model favors the occurrence of EADs because of the prolongation of APD_{90}, shown here for a CL of 1000 ms. This APD_{90} prolongation is caused by both I_{CaL} and I_{NaL}, which lengthen the plateau phase and allow the late calcium current to reactivate. When preventing I_{CaL} recovery or blocking I_{NaL} in the HF-OVVR model, EADs were suppressed.

F. Comparison With Previous HF Models

In this section, we compare HF biomarkers of the HF-OVVR model with previous HF simulation studies:

1) *AP duration at 90%:* APD_{90} in [8], 548.8 ms, increased by 46.7%; in [9], 273.0 ms, increased by 22.9%, 369.0 ms, increased by 44.1%, and 338.0 ms, increased by 50.2% for epicardial, midmyocardial, and endocardial cell types, respectively; in [10], ∼470.0 ms, increased by 24.0%; in [11], 500.0 ms, increased by 66.7%; in [12], 600.0 ms, increased by 106.9%; in [17], increased by ∼30.0%; in [20], increased by 562.5 ms; in [21], increased by ∼45.0%; in [22], increased by ∼ 400.0 ms for epicardial and endocardial cell types in one of their HF model; and in [23], 350.0 ms, increased by ∼18.0%. Two studies [16], [18] measured different repolarization thresholds; [16] calculated APD_{80} and had a population median increased by 19.6%, while [18] computed APD_{75} and found 215.0 ms increased by ∼30.0%. In our HF-OVVR model, the variability of parameters covers these APD prolongations, where APD_{90} increased within a range from 306.9 to 590.7 ms (33.6–157.2%), 392.8 to 628.8 ms (13.9–82.3%), and 352.2 to 512.2 ms (34.3–95.3%) for epicardial, midmyocardial, and endocardial cell types, respectively.
2) *AP duration at 50%:* Two studies [8], [10] quantified APD_{50}, where in [8] quantified APD_{50} with a measured value 374.5 ms, increased by 20.7%; in [10] increased by 18.0% from normal level. For the HF-OVVR model, the APD_{50} ranges were increased by 249.0–436.9 ms (32.7–132.9%), 318.3–466.4 ms (13.2–65.8%), and 277.7–373.1 ms (33.8—79.7%), for epicardial, midmyocardial, and endocardial cell types, respectively.
3) *AP triangulation:* For triangulation, a sole study [10] quantified it and found an increase of 43.0%. In our HF-OVVR model, the ranges are increased by 57.9–153.8 ms (37.5—265.3%), 74.5–162.4 ms (16.9–154.9%), and 74.5–139.1 ms (19.8–154.3%), for epicardial, midmyocardial, and endocardial cell types, respectively. In addition, Walmsley *et al.* [16] measured the median population and found an increase ranging between 7.0% and 10.0%.
4) *Calcium transient dynamics:* The peak value of $[\mathrm{Ca}^{2+}]_i$ was 334.0 nmol/L as reported by [8] with a reduction of 45.6% from the normal level. [12] found that the amplitude was 580.0 μM with a decrease of 22.7% from the normal peak. [10] measured that the amplitude was reduced by 41.0% from the normal model. Shannon *et al.* [17] found a reduction in the calcium peak levels under HF without quantifying it. Puglisi and Bers [18] found a decrease less than 40.0%. In our HF-OVVR model, the peak value of $[Ca^{2+}]_i$ falls within a range increased by 193.3–627.8, 255.7–793.6, and 267.5–352.3 μM, for epicardial, midmyocardial, and endocardial cell types, respectively. One study [12] measured the time to peak $[\mathrm{Ca}^{2+}]_i$ as 420.0 ms, increased by 460.0%, while our ranges increased by 44.7–175.5, 47.6–181.7, and 64.9–168.5 ms, for epicardial, midmyocardial, and endocardial cell types, respectively. The diastolic steady-state was reported by [8] with a value of 136.0 nmol/L increased by 13.3%; our HF-OVVR model obtains values of 82.1–89.3, 94.1–96.8, and 94.8–99.1μM,

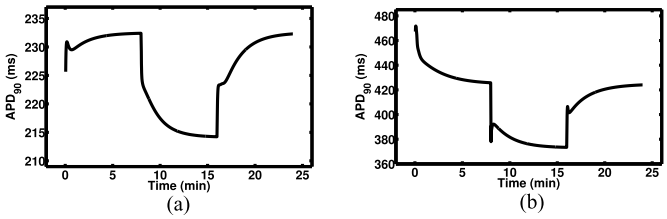

Fig. 5. Time course of APD accommodation after an abrupt change in CL for the (a) normal OVVR and (b) HF-OVVR model. The epicardial cell type was used.

for epicardial, midmyocardial, and endocardial cell types, respectively. The time to reach steady state for $[Ca^{2+}]_i$ is 630.0 ms, increased by 39.7%, as reported by [10]. Walmsley *et al.* [16] measured the median calcium transient peak value, duration, and triangulation for the whole population and found a reduction of 44.4%, increase of 51.7%, and reduction of 11.6%, respectively. Another study [21] found that $[Ca^{2+}]_{SR}$ under HF conditions is reduced by 15.0% in store because the restoring rate is slower.

5) *Sodium dynamics:* For $[Na^+]_i$ accumulation, Trenor *et al.* [10] observed an increase in levels compared with a normal model. Also, Moreno *et al.* [23] found that the intracellular sodium concentration level was 11.45 mM, increased by ∼28.7%. In our HF-OVVR model, the peak $[Na^+]_i$ values are increased by 2.6–15.6%, 6.1–15.9%, and 5.3–18.7% for epicardial, midmyocardial, and endocardial cells, respectively.
6) *Induction of EADs:* For EADs, only one HF simulation study [10] reported that EADs can be induced. As shown in Fig. 7, our HF-OVVR can induce EADs. Table III indicates the EADs CLs range and APD_{90} in the EADs regime for all cell types.

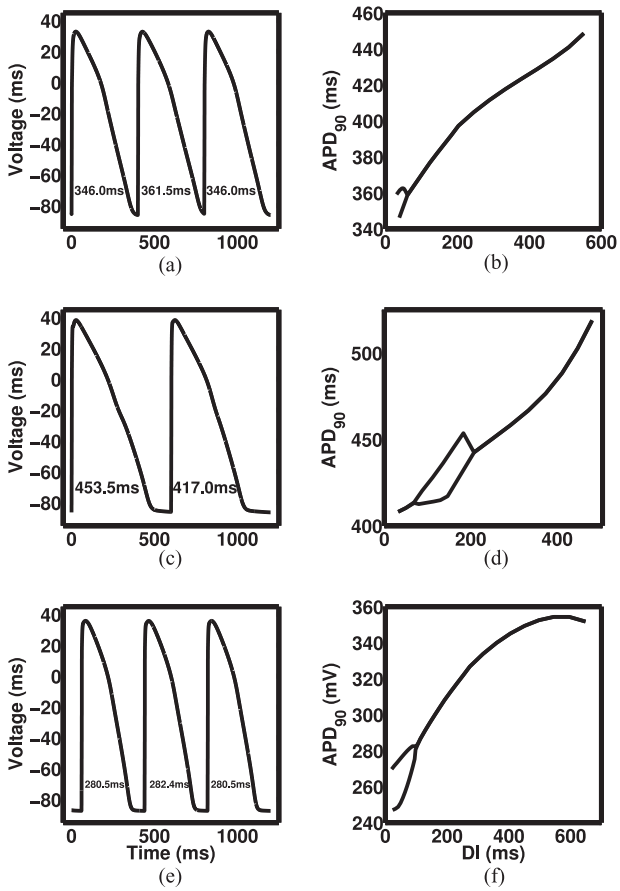

Fig. 6. ALTs in a single epicardial (first row), midmyocardial (second row), and endocardial (third row) cell from the HF-OVVR model. (a), (c), (e) AP traces. (b), (d), (f) Bifurcation.

V. Discussion

In this paper, we present a human HF model (HF-OVVR) derived from experimental observations on remodeling of ion channels mainly from human data and for comparison use the undiseased ventricular cell model (OVVR) [15]. Our new HF-OVVR model can reproduce many of the AP properties of failing human myocytes. We have compared the properties of the HF-OVVR model with available experimental observations and found good agreement. We have found that APD_{90} is prolonged by 77.2–361.0, 47.8–283.8, and 89.9–249.9 ms for epicardial, midmyocardial, and endocardial cells in our model, which agrees with experimental observations of ∼181 ± 28 ms prolongation for the HF case [45]. In addition, we found that APD_{50} is prolonged by 61.4–249.3, 37.0–185.1, and 70.1–165.5 ms during HF for epicardial, midmyocardial, and endocardial cells, which are close to experimental findings of ∼156 ± 22 ms at a CL of 2000 ms [45].

We defined AP triangulation as the difference between APD_{90} and APD_{50} and found that our simulated AP triangulation was comparable with experimental studies [37], [91]. Also, experiments showed a nonsignificant increase in the RMP ranging between 0.2 and 1.0 ms [92], which is in agreement with the 0.0–1.3, 0.1–1.8, and 0.1–1.4 ms increases in RMP for epicardial, midmyocardial, and endocardial cells in our HF-OVVR model.

In addition, the dynamics of simulated $[Ca^{2+}]_i$ match experimental findings, including decreased systolic amplitude (SA) range 10.0–72.3%, 23.0–75.2%, and 12.3–33.4% for epicardial, midmyocardial, and endocardial cells in our HF-OVVR model compared to a reduction of 41% in experiments [37], [93]. Also, previous experiments observed a slight increase in diastolic $[Ca^{2+}]_i$ [91], which matches our simulation results, which increased by 6.5–15.8%, 1.4–4.3%, and 8.5–13.4% for epicardial, midmyocardial, and endocardial cells, respectively. The difference between the SA of $[Ca^{2+}]_i$ in HF and normal cells has been observed to be 379 ± 140 nM [8], which is in the range of the difference observed for our HF-OVVR model of 69.6-504.1 and 237.4–775.3 nM for epicardial and midmyocardial cells. The difference of the upstroke time or time to peak for the Ca^{2+} transient is 20 ± 11 ms for a CL of 3000 ms [94], whereas in our HF-OVVR model, it is 3.2–134.0, 15.3–149.4, and 9.5–113.1 ms for epicardial, midmyocardial, and endocardial cells, respectively. $[Na^+]_i$ is increased in HF-OVVR cells for all stimulation rates when compared with the normal cell, which matches previous findings [95].

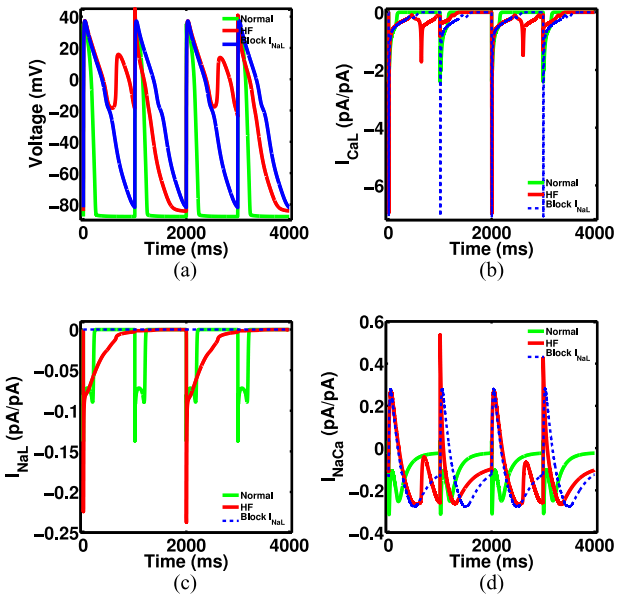

Fig. 7. Mechanisms for EADs of the HF-OVVR model for the epicardial cell type. (a) AP traces. (b) I_{CaL}. (c) I_{NaL}. (d) I_{NaCa} under normal (solid green lines), HF (solid red lines), and blocked I_{NaL} (dotted blue lines) with CL= 1000 ms.

Our approach includes some limitations. Recent work on mRNA [16] has shown that ALTs in human HF cells begins at a CL of 350 ms, whereas ALTs in our case is higher by 50, 250, and 30 ms for epicardial, midmyocardial, and endocardial cells, respectively. However, ALTs onset CLs are in the range of the observed values reported in other studies [96] of $\leq$500 ms for epicardial and endocardial cells. In addition, in our simulation results, we observed that the maximum range of APD S-S restitution curve slopes is 0.26–0.60, 0.23–0.70, and 0.28–0.86 for epicardial, midmyocardial, and endocardial cells, respectively. For epicardial and midmyocardial, it is less than the slope value of 0.86 $\pm$ 0.12 measured in the LV free wall of the failing human heart [3] for epicardial and midmyocardial cells, but it matches the measured endocardial cell.

In addition, to build the HF-OVVR model that was used in this paper, the experimental data come from various sources of previously published studies. The data for each study have various HF causes, and we do not have access to the raw data of these studies. Therefore, in our HF-OVVR simulations, we calculated the mean of the means of these studies and the SD as the square root of the squared sum of the variances of these studies. This would not represent uncertainty arising from different HF causes; instead, it is averaging of the variability within each of these studies across different HF causes.

On comparing our model with previous HF simulation models [8], [12], we found that many of those models did not reproduce as many of the properties of HF that are observed in a single human HF-remodeled myocyte, such as leveraged accumulated $[\mathrm{Na}^{+}]_i$, ALTs, and EADs. These models were designed to reproduce the two prominent properties: prolonged APD_{90} and altered $[\mathrm{Ca}^{2+}]_i$ dynamics. Also, these studies used more limited data and did not show most of the HF-remodeled properties in a quantitative manner. Most of the previous models, [8], [12], did not consider remodeling I_{Na} in reproducing the reduction in the upstroke velocity of HF cells. Also, these models either did not remodel the I_{NaL} [8] or increased it more than has been observed [12]. Moreover, previous simulation studies did not incorporate remodeling of I_{to} and I_{Kr}. Previous simulation studies [8], [12] did not change these currents. Regarding APD rate dependence, only one study [9] compared with control at a fast rate.

VI. Conclusion and Future Work

In the present study, first, a simulation study of an AP waveform of different ventricular cell types was presented based on recent experimental studies of transmural electrophysiological heterogeneities in the HF-OVVR model and compared with the normal OVVR model. Second, we evaluated how major cellular ionic currents influence the AP repolarization phase and how the APD rate dependence changed in transmural cells. Third, we found that these results are in good accordance with experimental findings reported in the literature and might motivate further research on remodeling and simulation of HF at both tissue and the whole organ levels. In conclusion, the HF-OVVR model established in this paper was mainly used to investigate the transmural electrophysiological heterogeneities of different ventricular cell types in failing human hearts. In future work, we intend to investigate our model's properties in tissue, including conduction velocity, and to determine how HF remodeling at the cellular level could affect the spatiotemporal dynamics of induced arrhythmias in realistic heart geometries. In addition, the inclusion of CaMK in the model will facilitate investigating how drug-induced alterations in ionic current and exchanger properties may modulate the electrophysiological properties in HF.

Acknowledgment

The authors are very grateful to Dr. Ernest Fokoue at Rochester Institute of Technology (RIT) for his valuable suggestions and assistance in preparing the statistical part of the manuscript.

References

[1] A. S. Go *et al.*, "Heart disease and stroke statistics—2014 update: A report from the American Heart Association," *Circulation*, vol. 128, pp. 00–00, 2013.
[2] R. Coronel *et al.*, "Electrophysiological changes in heart failure and their implications for arrhythmogenesis," *Biochimica et Biophysica Acta (BBA), Molecular Basis Disease*, vol. 1832, no. 12, pp. 2432–2441, 2013.
[3] A. V. Glukhov, "Transmural dispersion of repolarization in failing and nonfailing human ventricle," *Circulation Res.*, vol. 106, no. 5, pp. 981–991, 2010.
[4] Q. Lou *et al.*, "Transmural heterogeneity and remodeling of ventricular excitation-contraction coupling in human heart failure," *Circulation*, vol. 123, no. 17, pp. 1881–1890, 2011.
[5] M. Luo and M. E. Anderson, "Mechanisms of altered ca2+ handling in heart failure," *Circulation Res.*, vol. 113, no. 6, pp. 690–708, 2013.
[6] S. Nattel, *et al.*, "Arrhythmogenic ion-channel remodeling in the heart: Heart failure, myocardial infarction, and atrial fibrillation," *Physiol. Rev.*, vol. 87, no. 2, pp. 425–456, 2007.
[7] M. J. Cutler *et al.*, "Cardiac electrical remodeling in health and disease," *Trends Pharmacological Sci.*, vol. 32, no. 3, pp. 174–180, 2011.
[8] L. Priebe and D. J. Beuckelmann, "Simulation study of cellular electric properties in heart failure," *Circulation Res.*, vol. 82, no. 11, pp. 1206–1223, 1998.

[9] Y. Zhang *et al.*, "Simulation study of transmural cellular electrical properties in failed human heart," in *Proc. 27th Annu. Int. Conf. Eng. Med. Biol. Soc.*, Jan. 2005, pp. 337–340.

[10] B. Trenor *et al.*, "Simulation and mechanistic investigation of the arrhythmogenic role of the late sodium current in human heart failure," *PLoS ONE*, vol. 7, no. 3, p. e32659, Mar. 2012.

[11] R. L. Winslow *et al.*, "Mechanisms of altered excitation-contraction coupling in canine tachycardia-induced heart failure, ii: Model studies," *Circulation Res.*, vol. 84, no. 5, pp. 571–586, 1999.

[12] Y. Zang and L. Xia, " Electrical remolding and mechanical changes in heart failure: A model study," in *Life System Modeling and Intelligent Computing* (ser. Lecture Notes in Computer Science), vol. 6330, K. E. A. Li, Ed. Berlin, Germany: Springer, 2010, pp. 421–429.

[13] R. L. Winslow *et al.*, "Modeling the cellular basis of altered excitation-contraction coupling in heart failure," *Prog. Biophys. Molecular Biol.*, vol. 69, nos. 2/3, pp. 497–514, 1998.

[14] S. Zlochiver, "Subthreshold parameters of cardiac tissue in a bi-layer computer model of heart failure," *Cardiovasc. Eng.*, vol. 10, no. 4, pp. 190–200, 2010.

[15] T. O'Hara *et al.*, "Simulation of the undiseased human cardiac ventricular action potential: Model formulation and experimental validation," *PLoS Comput. Biol.*, vol. 7, no. 5, p. e1002061, May 2011.

[16] J. Walmsley *et al.*, "mRNA expression levels in failing human hearts predict cellular electrophysiological remodeling: A population-based simulation study," *PLoS ONE*, vol. 8, no. 2, p. e56359, Feb. 2013.

[17] T. R. Shannon *et al.*, "Regulation of cardiac sarcoplasmic reticulum Ca release by luminal [Ca] and altered gating assessed with a mathematical model," *Biophys. J.*, vol. 89, no. 6, pp. 4096–4110, 2005.

[18] J. L. Puglisi and D. M. Bers, "LabHEART: An interactive computer model of rabbit ventricular myocyte ion channels and Ca transport," *Am. J. Physiol., Cell Physiol.*, vol. 281, no. 6, pp. C2049–C2060, 2001.

[19] S. M. Narayan *et al.*, "Action potential dynamics explain arrhythmic vulnerability in human heart failure: A clinical and modeling study implicating abnormal calcium handling," *J. Am. College Cardiol.*, vol. 52, no. 22, pp. 1782–1792, 2008.

[20] J. D. Moreno *et al.*, "A computational model to predict the effects of class i anti-arrhythmic drugs on ventricular rhythms," *Sci. Translational Med.*, vol. 3, no. 98, p. 98ra83, 2011.

[21] L. Lu *et al.*, "Simulation of arrhythmogenic effect of rogue RyRs in failing heart by using a coupled model," *Comput. Math. Methods Med.*, vol. 9, p. e106602, 2012.

[22] J. F. Gomez *et al.*, "Electrophysiological and structural remodeling in heart failure modulate arrhythmogenesis. 1d simulation study," *PLoS ONE*, vol. 9, no. 9, p. e106602, Sep. 2014.

[23] J. D. Moreno *et al.*, "Ranolazine for congenital and acquired late INa-linked arrhythmias: In silico pharmacological screening," *Circulation Res.*, vol. 113, no. 7, pp. e50–e61, 2013.

[24] R. Huang *et al.*, "Cellular level electromechanical modeling and simulation of heart failure," in *Proc. 27th Annu. Int. Conf. Eng. Med. Biol. Soc.*, Jan. 2005, pp. 7301–7304.

[25] M. M. Elshrif *et al.*, "Electrophysiological properties under heart failure conditions in a human ventricular cell: A modeling study," in *Proc. 36th Annu. Int. Conf. Eng. Med. Biol. Soc.*, Aug. 2014, pp. 4324–4329.

[26] E. Soltysinska *et al.*, " Transmural expression of ion channels and transporters in human nondiseased and end-stage failing hearts," *Pflugers Arch.*, vol. 459, no. 1, pp. 11–23, 2009.

[27] J. Prestle *et al.*, "Heterogeneous transmural gene expression of calcium-handling proteins and natriuretic peptides in the failing human heart," *Cardiovasc. Res.*, vol. 43, no. 2, pp. 323–331, 1999.

[28] F. G. Akar and D. S. Rosenbaum, "Transmural electrophysiological heterogeneities underlying arrhythmogenesis in heart failure," *Circulation Res.*, vol. 93, no. 7, pp. 638–645, 2003.

[29] C. R. Valdivia *et al.*, "Increased late sodium current in myocytes from a canine heart failure model and from failing human heart," *J. Molecular Cellular Cardiol.*, vol. 38, no. 3, pp. 475–483, 2005.

[30] L. L. Shang *et al.*, "Human heart failure is associated with abnormal c-terminal splicing variants in the cardiac sodium channel," *Circulation Res.*, vol. 101, no. 11, pp. 1146–1154, 2007.

[31] G. Gao *et al.*, "Role of rbm25/luc7l3 in abnormal cardiac sodium channel splicing regulation in human heart failure," *Circulation*, vol. 124, no. 10, pp. 1124–1131, 2011.

[32] A. I. Undrovinas *et al.*, "Gating of the late Na^+ channel in normal and failing human myocardium," *J. Molecular Cellular Cardiol.*, vol. 34, no. 11, pp. 1477–1489, 2002.

[33] V. A. Maltsev and A. I. Undrovinas, "A multi-modal composition of the late Na^+ current in human ventricular cardiomyocytes," *Cardiovasc. Res.*, vol. 69, no. 1, pp. 116–127, 2006.

[34] V. A. Maltsev *et al.*, "Chronic heart failure slows late sodium current in human and canine ventricular myocytes: Implications for repolarization variability," *Eur. J. Heart Failure*, vol. 9, no. 3, pp. 219–227, 2007.

[35] R. P. Rasmussen *et al.*, "Calcium antagonist binding sites in failing and nonfailing human ventricular myocardium," *Biochem. Pharmacol.*, vol. 39, no. 4, pp. 691–696, 1990.

[36] D. J. Beuckelmann *et al.*, "Characteristics of calcium-current in isolated human ventricular myocytes from patients with terminal heart failure," *J. Molecular Cellular Cardiol.*, vol. 23, no. 8, pp. 929–937, 1991.

[37] D. Beuckelmann and E. Erdmann, "Ca(2+)-currents and intracellular $[Ca^{2+}]_i$-transients in single ventricular myocytes isolated from terminally failing human myocardium," *Basic Res. Cardiol.*, vol. 87, no. Suppl 1, pp. 235–243, 1992.

[38] T. Mewes and U. Ravens, "L-type calcium currents of human myocytes from ventricle of non-failing and failing hearts and from atrium," *J. Molecular Cellular Cardiol.*, vol. 26, no. 10, pp. 1307–1320, 1994.

[39] G. F. Tomaselli *et al.*, "Sudden cardiac death in heart failure. the role of abnormal repolarization." *Circulation*, vol. 90, no. 5, pp. 2534–2539, 1994.

[40] H. Ouadid *et al.*, "Calcium currents in diseased human cardiac cells," *J. Cardiovasc. Pharmacol.*, vol. 25, no. 2, pp. 282–291, 1995.

[41] F. Schröder *et al.*, "Increased availability and open probability of single l-type calcium channels from failing compared with nonfailing human ventricle," *Circulation*, vol. 98, no. 10, pp. 969–976, 1998.

[42] S. Kääb *et al.*, "Molecular basis of transient outward potassium current downregulation in human heart failure: A decrease in Kv4.3 mRNA correlates with a reduction in current density," *Circulation*, vol. 98, no. 14, pp. 1383–1393, 1998.

[43] R. Schwinger *et al.*, "Regional expression and functional characterization of the l-type Ca2+-channel in myocardium from patients with end-stage heart failure and in non-failing human hearts," *J. Molecular Cellular Cardiol.*, vol. 31, no. 1, pp. 283–296, 1999.

[44] X. Chen *et al.*, "L-type Ca2+ channel density and regulation are altered in failing human ventricular myocytes and recover after support with mechanical assist devices," *Circulation Res.*, vol. 91, no. 6, pp. 517–524, 2002.

[45] L. Gui-Rong *et al.*, "Ionic current abnormalities associated with prolonged action potentials in cardiomyocytes from diseased human right ventricles," *Heart Rhythm*, vol. 1, no. 4, pp. 460–468, 2004.

[46] D. J. Beuckelmann *et al.*, "Alterations of k+ currents in isolated human ventricular myocytes from patients with terminal heart failure," *Circulation Res.*, vol. 73, no. 2, pp. 379–385, 1993.

[47] M. Näbauer *et al.*, "Characteristics of transient outward current in human ventricular myocytes from patients with terminal heart failure," *Circulation Res.*, vol. 73, no. 2, pp. 386–394, 1993.

[48] E. Wettwer *et al.*, "Transient outward current in human ventricular myocytes of subepicardial and subendocardial origin." *Circulation Res.*, vol. 75, no. 3, pp. 473–82, 1994.

[49] M. Näbauer *et al.*, "Regional differences in current density and rate-dependent properties of the transient outward current in subepicardial and subendocardial myocytes of human left ventricle," *Circulation*, vol. 93, no. 1, pp. 168–177, 1996.

[50] K. M. Holzem and I. R. Efimov, "Arrhythmogenic remodelling of activation and repolarization in the failing human heart," *Europace*, vol. 14, no. suppl 5, pp. v50–v57, 2012.

[51] T. Takahashi *et al.*, "Expression of dihydropyridine receptor (Ca2+ channel) and calsequestrin genes in the myocardium of patients with end-stage heart failure," *J. Clin. Investigation*, vol. 90, no. 3, pp. 927–935, Sep. 1992.

[52] S. Koumi *et al.*, "Characterization of inwardly rectifying k^+ channel in human cardiac myocytes: Alterations in channel behavior in myocytes isolated from patients with idiopathic dilated cardiomyopathy," *Circulation*, vol. 92, no. 2, pp. 164–174, 1995.

[53] M. J. Janse, "Electrophysiological changes in heart failure and their relationship to arrhythmogenesis," *Cardiovasc. Res.*, vol. 61, no. 2, pp. 208–217, 2004.

[54] F. G. Akar *et al.*, "Molecular mechanisms underlying k+ current down-regulation in canine tachycardia-induced heart failure," *Am. J. Physiol., Heart Circulatory Physiol.*, vol. 288, no. 6, pp. H2887–H2896, 2005.

[55] Y. Tsuji *et al.*, "Pacing-induced heart failure causes a reduction of delayed rectifier potassium currents along with decreases in calcium and transient outward currents in rabbit ventricle," *Cardiovasc. Res.*, vol. 48, no. 2, pp. 300–309, 2000.

[56] J. Rose *et al.*, "Molecular correlates of altered expression of potassium currents in failing rabbit myocardium," *Am. J. Physiol., Heart Circulatory Physiol.*, vol. 288, no. 5, pp. H2077–H2087, 2005.
[57] G.-R. Li *et al.*, "Transmural action potential and ionic current remodeling in ventricles of failing canine hearts," *Am. J. Physiol., Heart Circulatory Physiol.*, vol. 283, no. 3, pp. H1031–H1041, 2002.
[58] R. Studer *et al.*, "Gene expression of the cardiac Na^+-Ca^{2+} exchanger in end-stage human heart failure," *Circulation Res.*, vol. 75, no. 3, pp. 443–453, 1994.
[59] M. Flesch *et al.*, "Evidence for functional relevance of an enhanced expression of the Na^+-Ca^{2+} exchanger in failing human myocardium," *Circulation*, vol. 94, no. 5, pp. 992–1002, 1996.
[60] H. Reinecke *et al.*, "Cardiac Na+/Ca2+ exchange activity in patients with end-stage heart failure," *Cardiovasc. Res.*, vol. 31, no. 1, pp. 48–54, 1996.
[61] G. Hasenfuss *et al.*, "Relationship between Na+-Ca2+-exchanger protein levels and diastolic function of failing human myocardium," *Circulation*, vol. 99, no. 5, pp. 641–648, 1999.
[62] K. Kjeldsen *et al.*, "Na+,k+-atpase concentration in rodent and human heart and skeletal muscle: Apparent relation to muscle performance," *Cardiovasc. Res.*, vol. 22, no. 2, pp. 95–100, 1988.
[63] A. Nørgaard *et al.*, "Relation of left ventricular function and Na^+-k^+ pump concentration in suspected idiopathic dilated cardiomyopathy," *Am. J. Cardiol.*, vol. 61, no. 15, p. 1312–1315, 1988.
[64] R. H. G. Schwinger *et al.*, "Reduced sodium pump α_1, α_3, and β_1-isoform protein levels and Na+,k+-atpase activity but unchanged Na+-Ca2+ exchanger protein levels in human heart failure," *Circulation*, vol. 99, no. 16, pp. 2105–2112, 1999.
[65] R. H. Schwinger *et al.*, "Effectiveness of cardiac glycosides in human myocardium with and without downregulated beta-adrenoceptors," *J. Cardiovasc. Pharmacol.*, vol. 15, no. 5, p. 6927, 1990.
[66] O. I. Shamraj *et al.*, "Characterisation of na^+-k^+-atpase, its isoforms, and the inotropic response to ouabain in isolated failing human hearts," *Cardiovasc. Res.*, vol. 27, no. 12, pp. 2229–2237, 1993.
[67] J. J. Mercadier *et al.*, "Altered sarcoplasmic reticulum Ca2(+)-atpase gene expression in the human ventricle during end-stage heart failure." *J. Clinical Investigation*, vol. 85, no. 1, pp. 305–309, Jan. 1990.
[68] G. Hasenfuss *et al.*, " Calcium cycling proteins and force–frequency relationship in heart failure," *Basic Res. Cardiol.*, vol. 91, no. 1, pp. 17–22, 1996.
[69] M. Arai *et al.*, "Alterations in sarcoplasmic reticulum gene expression in human heart failure. A possible mechanism for alterations in systolic and diastolic properties of the failing myocardium." *Circulation Res.*, vol. 72, no. 2, pp. 463–469, 1993.
[70] K. Dipla *et al.*, "The sarcoplasmic reticulum and the na+/ca2+ exchanger both contribute to the Ca2+ transient of failing human ventricular myocytes," *Circulation Res.*, vol. 84, no. 4, pp. 435–444, 1999.
[71] G. Hasenfuss and B. Pieske, "Calcium cycling in congestive heart failure," *J. Molecular Cellular Cardiol.*, vol. 34, no. 8, pp. 951–969, 2002.
[72] T. Yamamoto *et al.*, "Abnormal Ca2+ release from cardiac sarcoplasmic reticulum in tachycardia-induced heart failure," *Cardiovasc. Res.*, vol. 44, no. 1, pp. 146–155, 1999.
[73] M. T. Jiang *et al.*, "Abnormal Ca2+ release, but normal ryanodine receptors, in canine and human heart failure," *Circulation Res.*, vol. 91, no. 11, pp. 1015–1022, 2002.
[74] V. Piacentino *et al.*, "Cellular basis of abnormal calcium transients of failing human ventricular myocytes," *Circulation Res.*, vol. 92, no. 6, pp. 651–658, 2003.
[75] Y. Sakakibara *et al.*, "Sodium current in isolated human ventricular myocytes," *Am. J. Physiol., Heart Circulatory Physiol.*, vol. 265, no. 4, pp. H1301–H1309, 1993.
[76] V. A. Maltsev *et al.*, "Novel, ultraslow inactivating sodium current in human ventricular cardiomyocytes," *Circulation*, vol. 98, no. 23, pp. 2545–2552, 1998.
[77] S. Zicha *et al.*, "Transmural expression of transient outward potassium current subunits in normal and failing canine and human hearts," *J. Physiol.*, vol. 561, no. 3, pp. 735–748, 2004.
[78] C. Zobel *et al.*, "Molecular dissection of the inward rectifier potassium current (i_{K1}) in rabbit cardiomyocytes: Evidence for heteromeric coassembly of Kir2.1 and Kir2.2," *J. Physiol.*, vol. 550, no. 2, pp. 365–372, 2003.
[79] S. Kääb *et al.*, "Ionic mechanism of action potential prolongation in ventricular myocytes from dogs with pacing-induced heart failure," *Circulation Res.*, vol. 78, no. 2, pp. 262–273, 1996.
[80] E. Watanabe *et al.*, "Upregulation of KCNE1 induces QT interval prolongation in patients with chronic heart failure," *Circulation J.*, vol. 71, no. 4, pp. 471–478, 2007.
[81] R. Studer *et al.*, " Expression and function of the cardiac Na+/Ca2+ exchanger in postnatal development of the rat, in experimentaliduced cardiac hypertrophy and in the failing human heart," *Basic Res. Cardiol.*, vol. 92, no. 1, pp. 53–58, 1997.
[82] P. D. Allen *et al.*, "Na(+)-channel activators increase cardiac glycoside sensitivity in failing human myocardium," *Basic Res. Cardiol*, vol. 87, no. Suppl 1, p. 8794, 1992.
[83] E. M. Cherry and F. H. Fenton, "A tale of two dogs: analyzing two models of canine ventricular electrophysiology," *Am. J. Physiol., Heart Circulatory Physiol.*, vol. 292, no. 1, pp. H43–H55, 2007.
[84] E. Pueyo *et al.*, "Characterization of QT interval adaptation to RR interval changes and its use as a risk-stratifier of arrhythmic mortality in amiodarone-treated survivors of acute myocardial infarction," *IEEE Trans. Biomed. Eng.*, vol. 51, no. 9, pp. 1511–1520, Sep. 2004.
[85] C. P. Lau *et al.*, "Hysteresis of the ventricular paced QT interval in response to abrupt changes in pacing rate," *Cardiovasc. Res.*, vol. 22, no. 1, pp. 67–72, 1988.
[86] M. R. Franz *et al.*, "Cycle length dependence of human action potential duration in vivo. effects of single extrastimuli, sudden sustained rate acceleration and deceleration, and different steady-state frequencies," *J. Clinical Investigation*, vol. 82, no. 3, pp. 972–979, 1988.
[87] M. M. Elshrif and E. M. Cherry, "A quantitative comparison of the behavior of human ventricular cardiac electrophysiology models in tissue," *PLoS ONE*, vol. 9, no. 1, p. e84401, Jan. 2014.
[88] S. Rush and H. Larsen, "A practical algorithm for solving dynamic membrane equations," *IEEE Trans. Biomed. Eng.*, vol. BME-25, no. 4, pp. 389–392, Jul. 1978.
[89] A. L. Hodgkin and A. F. Huxley, " A quantitative description of membrane current and its application to conduction and excitation in nerve," *Bull. Math. Biol.*, vol. 52, no. 1–2, pp. 25–71, 1990.
[90] A. Gorgels *et al.*, "Ventricular arrhythmias in heart failure," *Am. J. Cardiol.*, vol. 70, no. 10, p. 37C43C, 1992.
[91] D. J. Beuckelmann *et al.*, "Intracellular calcium handling in isolated ventricular myocytes from patients with terminal heart failure." *Circulation*, vol. 85, no. 3, pp. 1046–1055, 1992.
[92] Y. A. Kuryshev *et al.*, "Decreased sodium and increased transient outward potassium currents in iron-loaded cardiac myocytes: Implications for the arrhythmogenesis of human siderotic heart disease," *Circulation*, vol. 100, no. 6, pp. 675–683, 1999.
[93] C. R. Weber *et al.*, "Dynamic regulation of sodium/calcium exchange function in human heart failure," *Circulation*, vol. 108, no. 18, pp. 2224–2229, 2003.
[94] J. K. Gwathmey *et al.*, "Abnormal intracellular calcium handling in myocardium from patients with end-stage heart failure." *Circulation Res.*, vol. 61, no. 1, pp. 70–76, 1987.
[95] D. M. Bers, *Excitation-Contraction Coupling and Cardiac Contractile Force*. Dordrecht, The Netherlands: Kluwer, 2001.
[96] L. D. Wilson *et al.*, "Heart failure enhances susceptibility to arrhythmogenic cardiac alternans," *Heart Rhythm*, vol. 6, no. 2, pp. 251–259, 2009.

Mohamed Elshrif received the B.Sc. degree in computer engineering from Al-Fateh University, Tripoli, Libya, in 2000, and the MBA degree from Arab Academy, Banking, and Financial Sciences, Cairo, Egypt, in 2004. He is currently working toward the Ph.D. degree with the Rochester Institute of Technology, Rochester, New York, NY, USA.

His current research interests include cellular modeling of cardiac electrophysiology and machine learning techniques for the development and implementation of electrical activity of the heart.

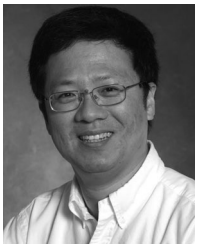

Pengcheng Shi received the B.S. degree in biomedical engineering from Shanghai Jiao Tong University, Shanghai, China, in 1989, and the M.S., M.Phil., and Ph.D. degrees in electrical engineering from Yale University, New Haven, CT, in 1992, 1993, and 1996, respectively.

He has been a Professor and the Director of the Ph.D. Program in Computing and Information Sciences, Rochester Institute of Technology since 2007. Previously, he had held faculty and leadership positions at Yale University (diagnostic radiology), New Jersey Institute of Technology (computer science), Hong Kong University of Science and Technology (electrical engineering and bioengineering), and Southern Medical University (biomedical engineering). His current research focus has been 2 on data-driven integrative system paradigms to biomedical imaging, image computing and intervention, computational physiology, and computational cognitive sciences.

Elizabeth Cherry received the Ph.D. degree in computer science from Duke University, Durham, NC, USA.

She held research positions at the Cornell University College of Veterinary Medicine, the Hofstra University Department of Physics, and the UCLA School of Medicine before joining the School of Mathematical Sciences, Rochester Institute of Technology, where she is an Associate Professor. Her main interests include mathematical modeling of cardiac electrophysiology at the subcellular, cellular, and tissue levels and computational methods for efficient numerical solution of these models.